

# Towards Efficient IACT Calibration with Deep learning-based Muon Identification

Robert Sturm  
Kameswara Mantha  
Lucy Fortson

## Project Goals

- Create a pipeline on Minnesota Supercomputing Institute (MSI) to be used for VERITAS calibration.
- Implement the Muon identification CNN proposed by Flanagan and train it on ~600K Muon Hunter images.
- Determine whether a simpler CNN architecture can produce equivalent model performance.
- Develop a muon fitting algorithm to determine a muon's centroid and radius.
- Determine whether or not the pipeline can identify more calibration-suitable muons than the existing method.

## Extensive Air Showers

- Extensive air showers** are initiated by an extraterrestrial very energetic particle entering the earth's atmosphere.
- Gamma-ray** induced air showers result in a cascade of pair production (creation of electron positron pairs) -> gamma-ray -> pair production -> ...
- Hadron** induced air showers result in a more complex cascade. Of relevance here is that:
  - Muons** are produced
  - Typically considered background, muons can be used for **calibration** of the telescope optics.
  - Cherenkov radiation** is light produced from charged particles traveling faster than the speed of light in a given medium.

Sources: [1][2][3]

## Imaging Atmospheric Cherenkov Telescopes (IACTs)

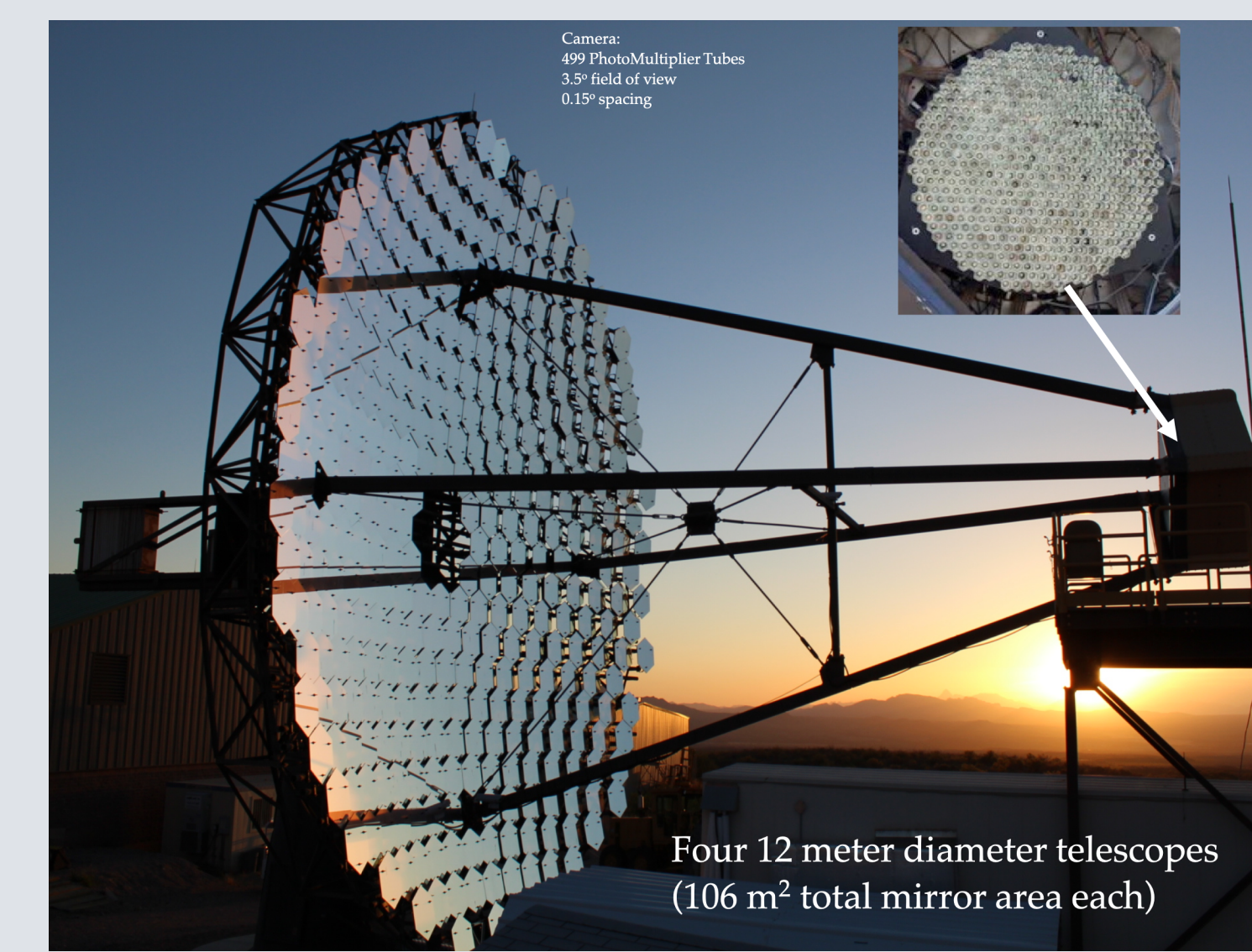


Figure 1: A VERITAS IACT. The telescope mirror reflects electromagnetic radiation to the camera, where the photomultiplier tubes (PMTs) reside. The PMTs capture the electromagnetic signal from Cherenkov radiation.

IACTs capture the electromagnetic signal from Cherenkov radiation within Extensive Air Showers.

### VERITAS

- We use images from the Very Energetic Radiation Imaging Telescope Array System (VERITAS) as data for our pipeline.
- VERITAS is an array of four IACTs located at the Fred Lawrence Whipple Observatory in southern Arizona.
- Each of the four telescopes is equipped with a 499-pixel PMT camera covering a field of view of 3.5°

## Gamma-ray Image

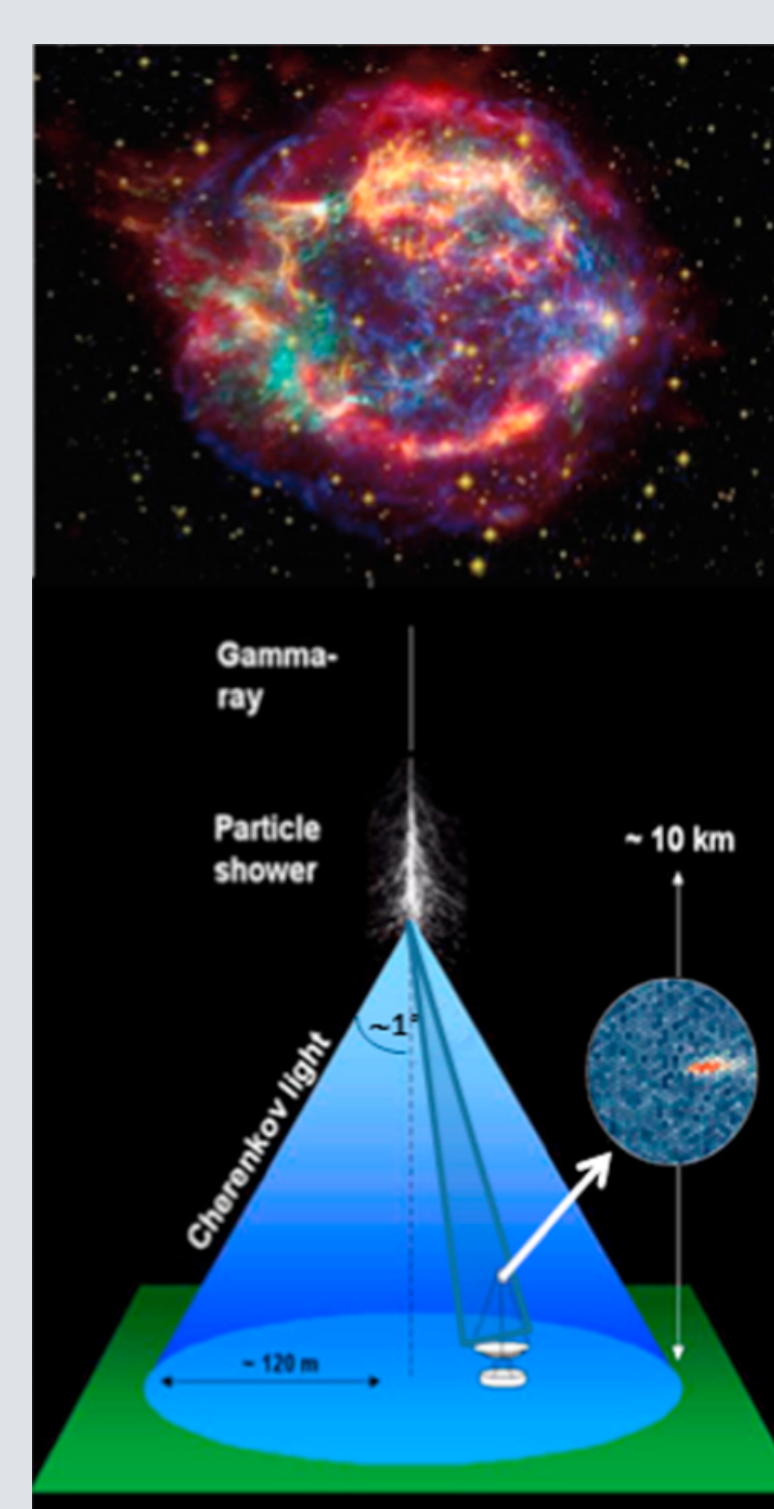


Figure 2: A gamma-ray induced air shower and resulting IACT image

IACTs were created for gamma-ray astronomy

Source: [4]

## IACT Calibration

- Measured electromagnetic values in muon images can be compared to expected theoretical values to perform instrumental calibration.
- The **impact parameter ( $\rho_R$ )** of a muon represents the distance between the camera axis and the trajectory of the muon.
- The size of an image is the sum of electromagnetic signal across all PMTs.
- IACTs can be calibrated using the **Cherenkov Angle ( $\theta$ )** and **impact-corrected size ( $i\_size$ )** from muon images.  $U_0^{PE}$  represents the calibration factor, used for instrument calibration.

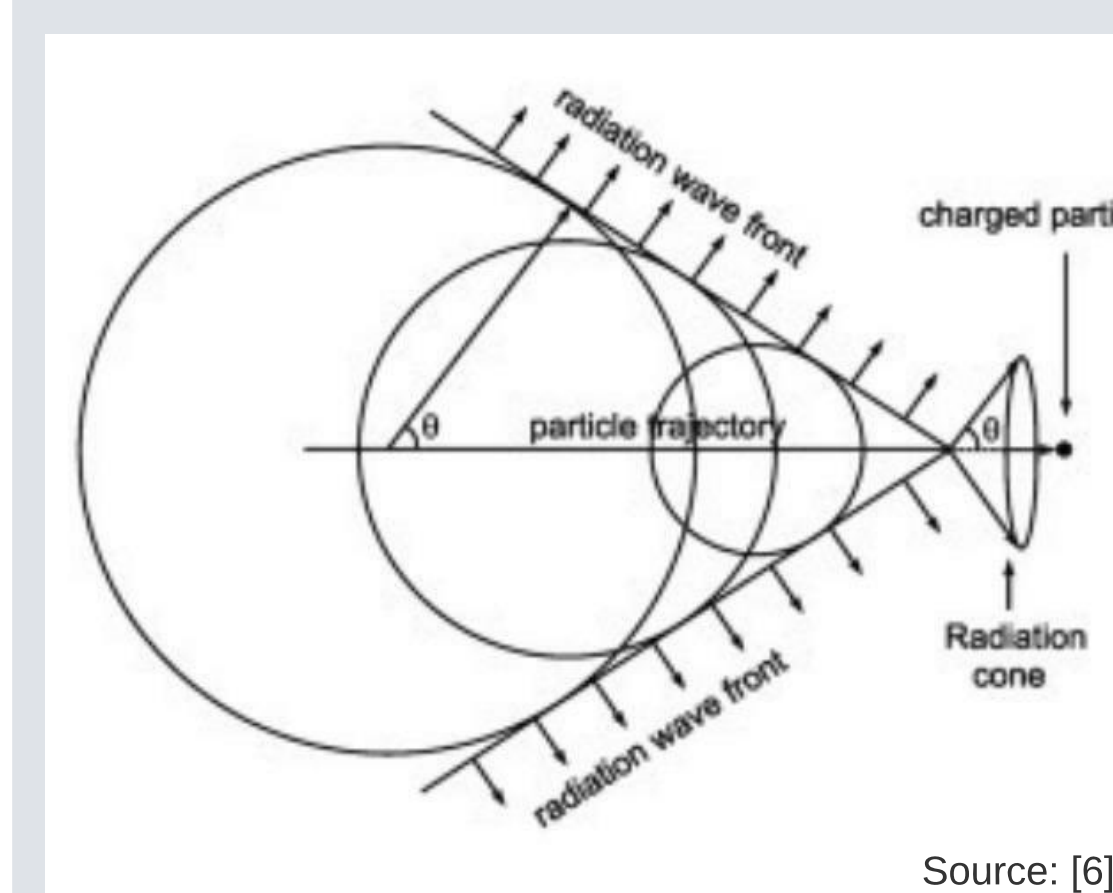


Figure 3: Cherenkov light emitted from a charged particle traveling faster than the speed of light in a medium.  $\theta$  represents the Cherenkov angle for the particle.

$$i\_size = \frac{\text{size}}{E_0(\rho_R)}$$

Equation 1: Impact-corrected size

$$U_0^{PE} = \frac{i\_size}{\Theta}$$

Equation 2: Calibration factor used for instrument calibration

Source: [2]

- The Muon Hunters projects on the Zooniverse.org platform provide classification labels - muon or not - for the VERITAS images.
- ~600K labeled images used to train the CNN.

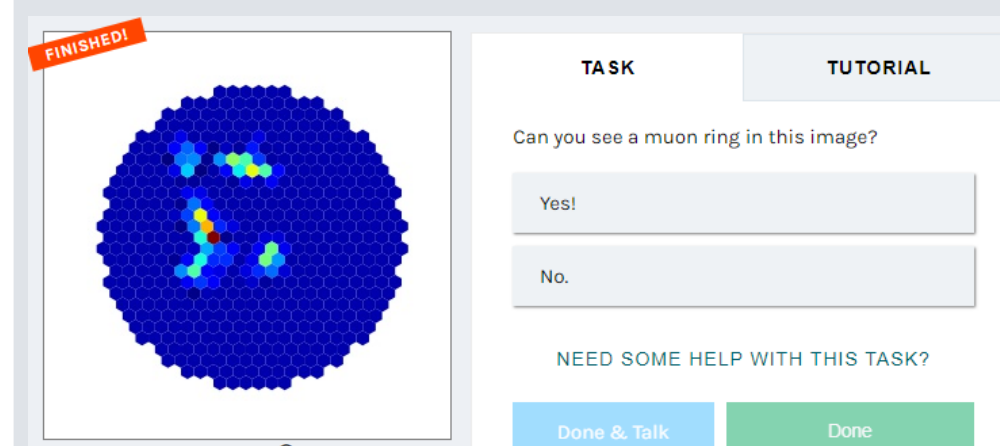
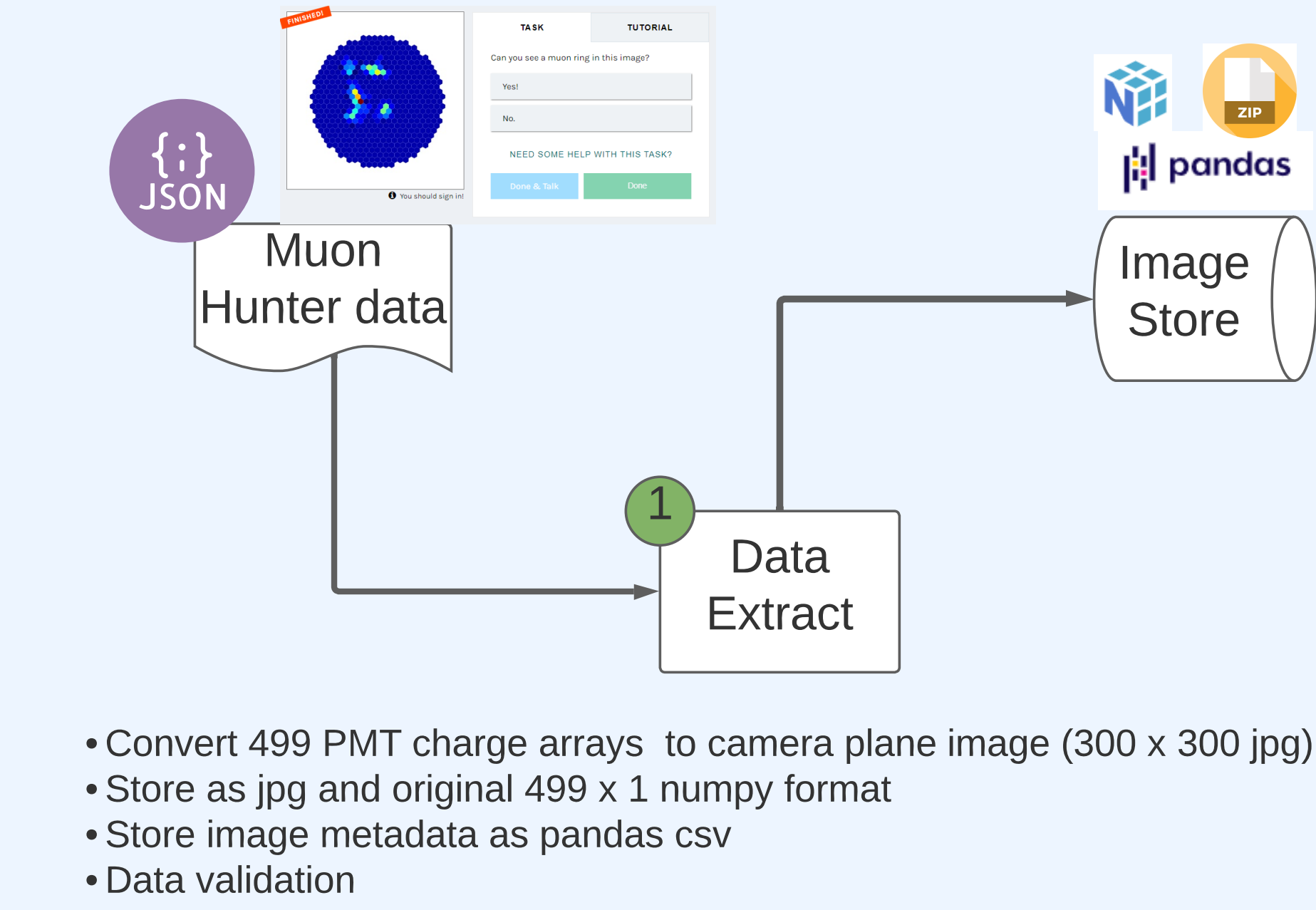


Figure 5: Dialogue shown in the Muon Hunters projects.

## Training & Telescope Calibration Pipelines



- Convert 499 PMT charge arrays to camera plane image (300 x 300 jpg)
- Store as jpg and original 499 x 1 numpy format
- Store image metadata as pandas csv
- Data validation

- Convert raw images to interpolated images (optional)
- Convert vote fractions to labels
- Normalize data
- Class balancing (optional)
- Train, validation, test splits
- Partition images, labels and ids into blocks
- Data validation
- Block partition data for streaming (for training)

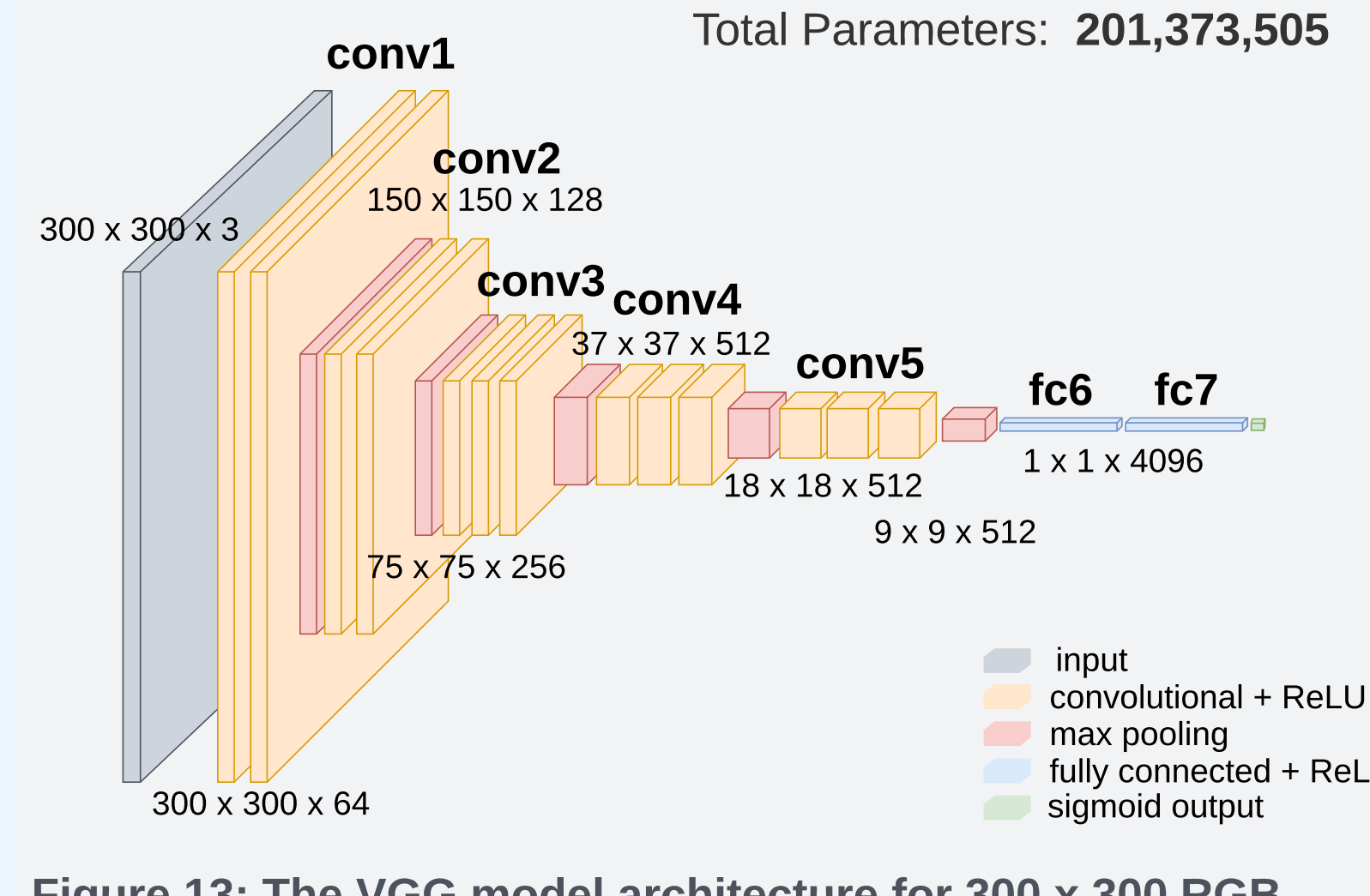
### Test dataset

- Train using 1 of 3 CNN models
- Save best model based on validation accuracy
- Log loss and accuracy history

### Model

- Create confusion matrix and calculate accuracy and FPR against test dataset.
- Create samples from each quadrant in confusion matrix.

### Test

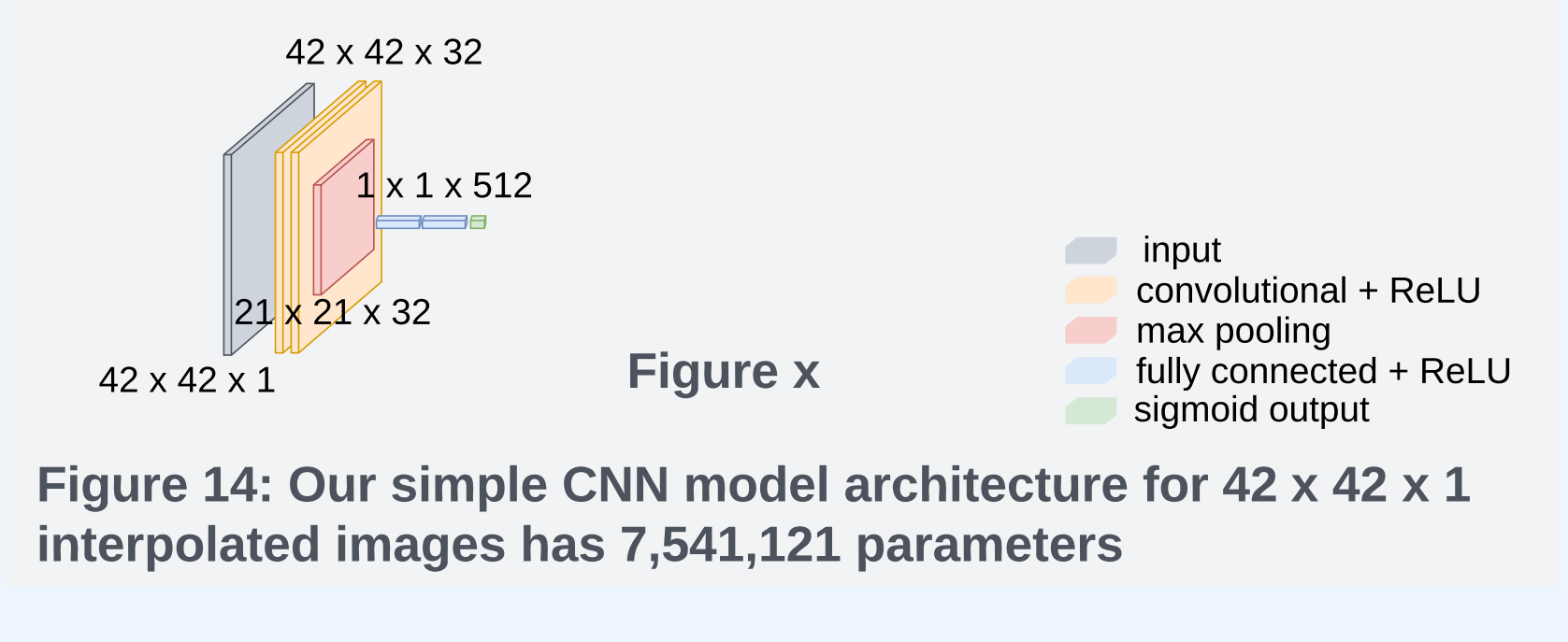


Total Parameters: 201,373,505

input convolutional + ReLU  
max pooling  
fully connected + ReLU  
sigmoid output

Figure 13: The VGG model architecture for 300 x 300 RGB images has 201,373,505 parameters

Total Parameters: 7,541,121



Total Parameters: 7,541,121

input convolutional + ReLU  
max pooling  
fully connected + ReLU  
sigmoid output

Figure 14: Our simple CNN model architecture for 42 x 42 x 1 interpolated images has 7,541,121 parameters

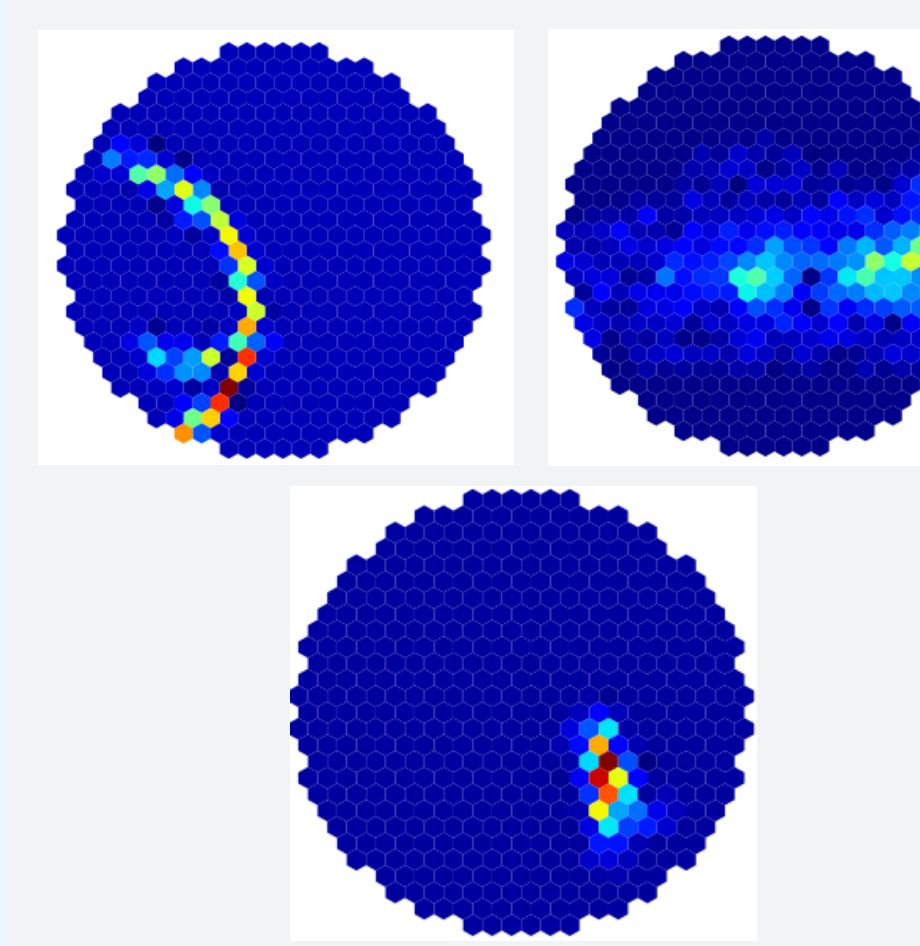


Figure 6: Images rendered using the camera plane visualization method used in Muon Hunters projects.

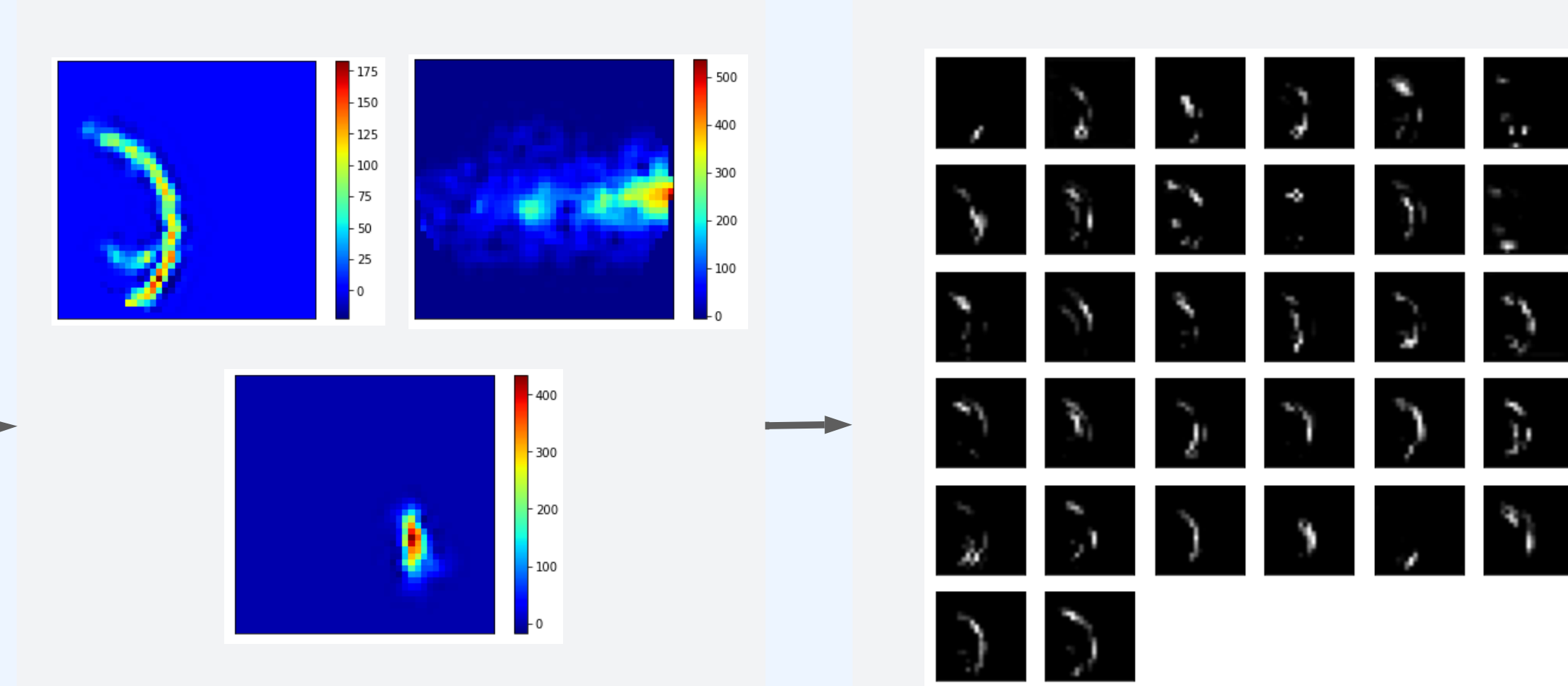


Figure 7: Image renderings for 42 x 42 x 1 interpolated images.

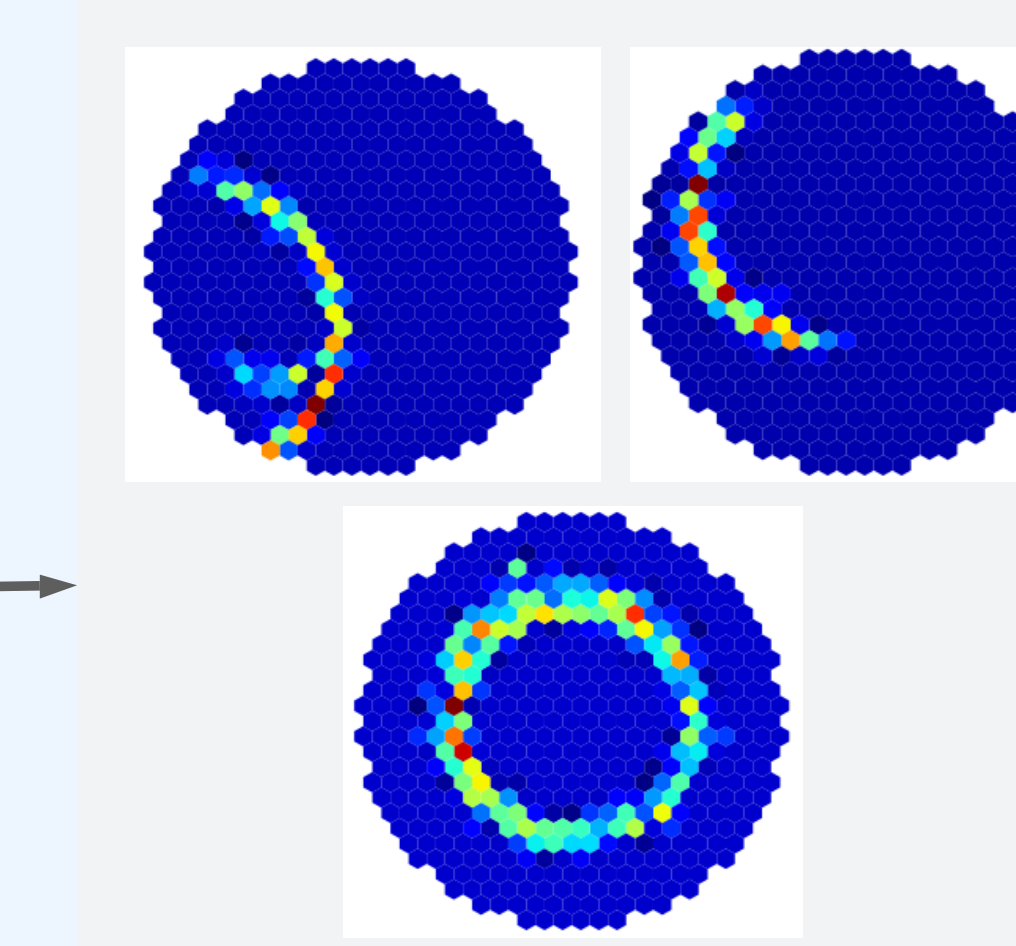


Figure 8: Image renderings for the 32 channels from the max pooling layer output of a truncated muon.

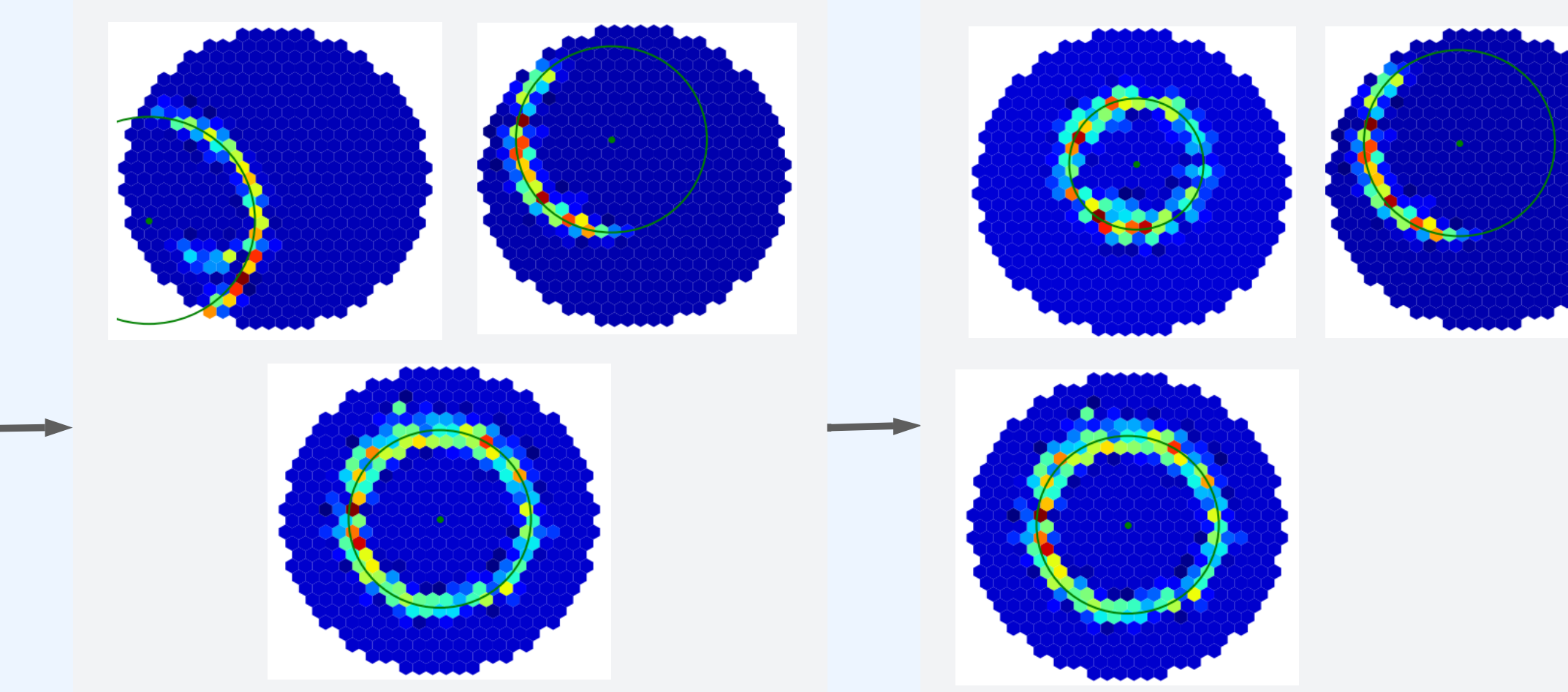


Figure 9: Images identified as containing a muon by the trained simple CNN.

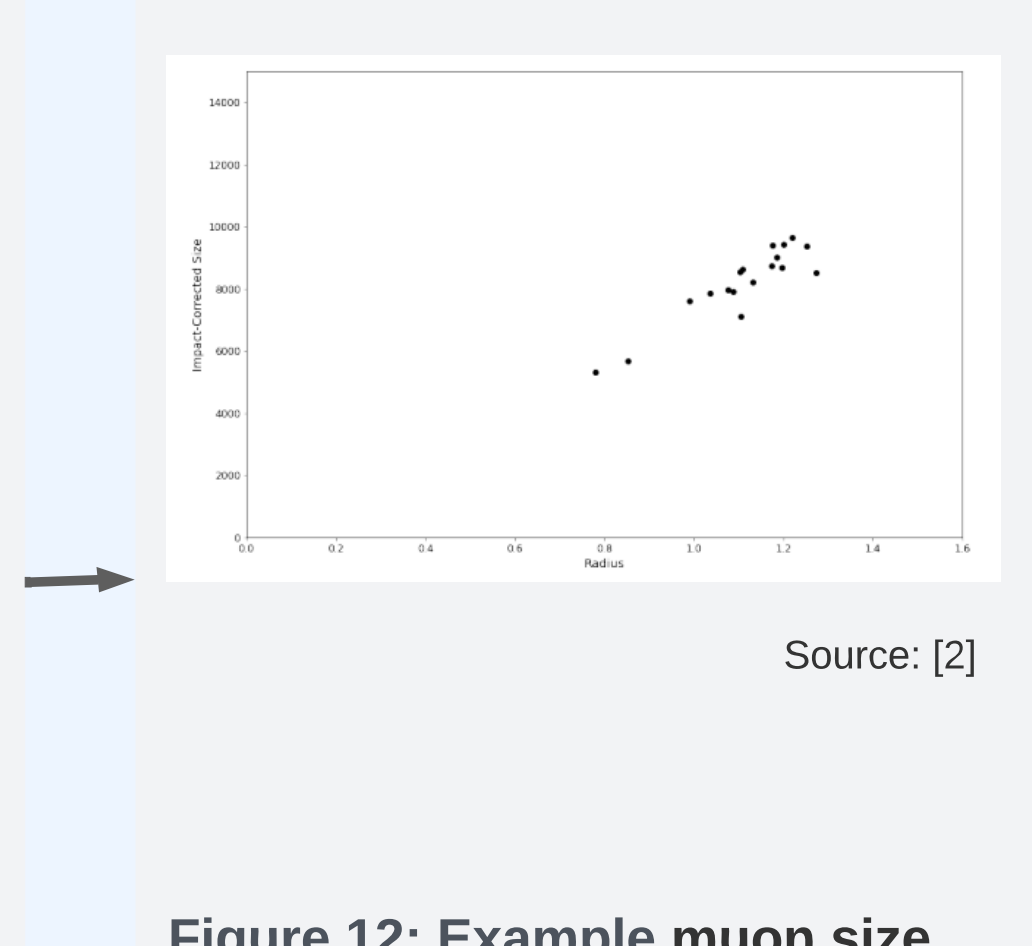


Figure 10: Muon images with ring fitting results superimposed.

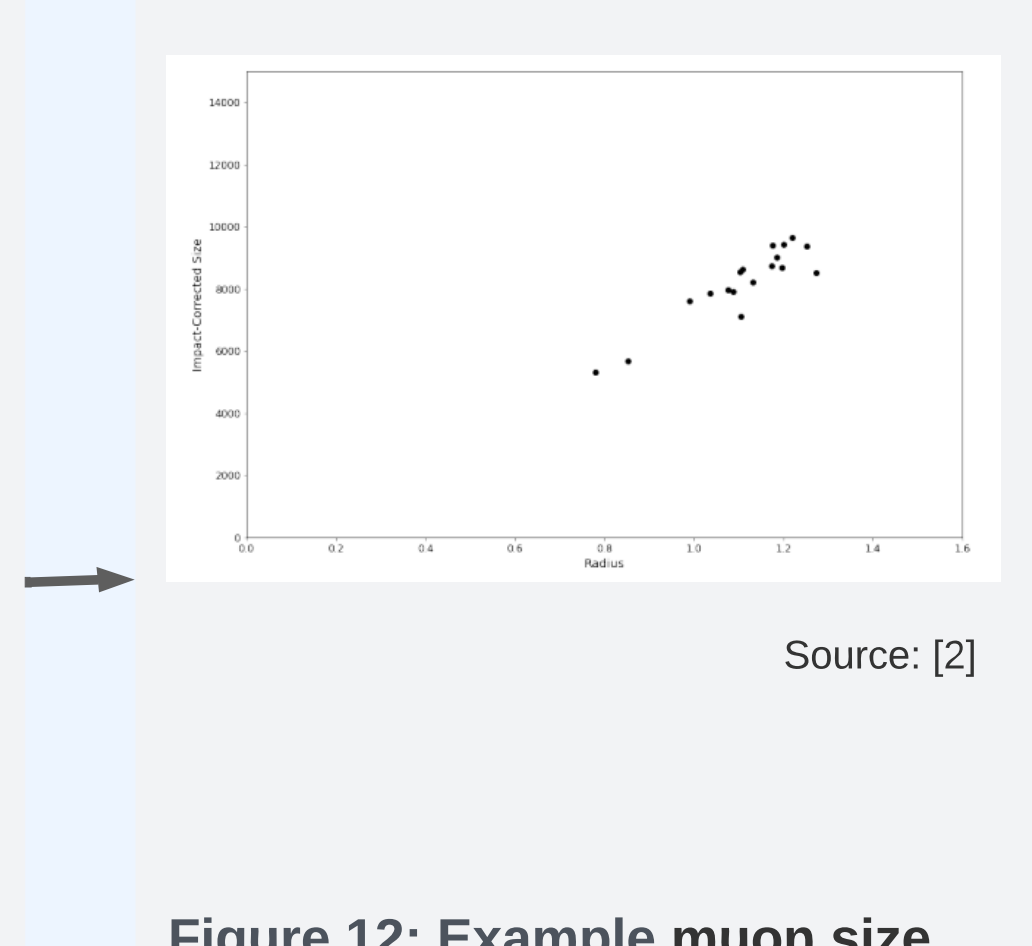


Figure 11: Muon images suitable for calibration.

Figure 12: Example muon size vs. radius plot used to predict the calibration factor.

## Muon Fitting Algorithm

- Zero-out all pixel values with negative value.
- Zero-out low pixel values. This is done by creating a histogram of  $n$  bins and truncating the lowest  $m$  bins.  $n$  and  $m$  are parameters.
- Set all pixels with value greater than the  $y$ th percentile to the  $y$ th percentile value.
- For each  $\sigma$  within a specified range:
  - Initialize centroid location to be  $(x_\mu, y_\mu)$ , the mean coordinates of the non-zero pixels.
  - Using a minimization algorithm, (we used Sequential Least Squares Programming), perturb the location of the centroid until a minimum cost is achieved for the current  $\sigma$  value. Our cost function uses a weighted least squares on the set of all distances from centroid to non-zero pixels within the current  $\sigma$  range. This eliminates or reduces the distortion of non-muon ring signal.
  - Return the radius and ring with the lowest cost.

Algorithm 1: Given a camera image identified as containing a muon, this algorithm will fit a centroid and radius to the muon ring segment within the image.

## CNN Results

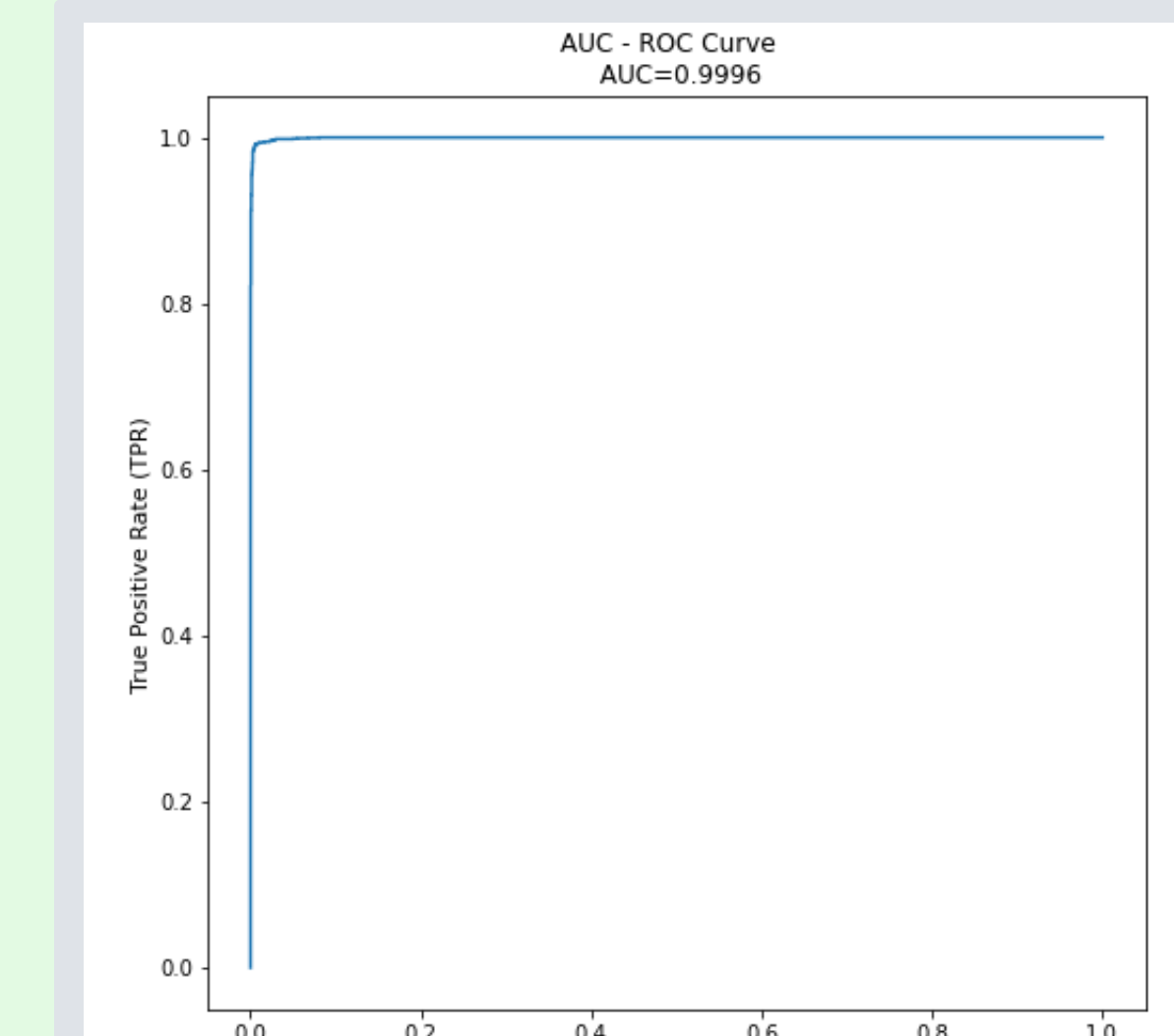


Figure 15: Area Under the Curve Receiver Operating Characteristics for our simple CNN

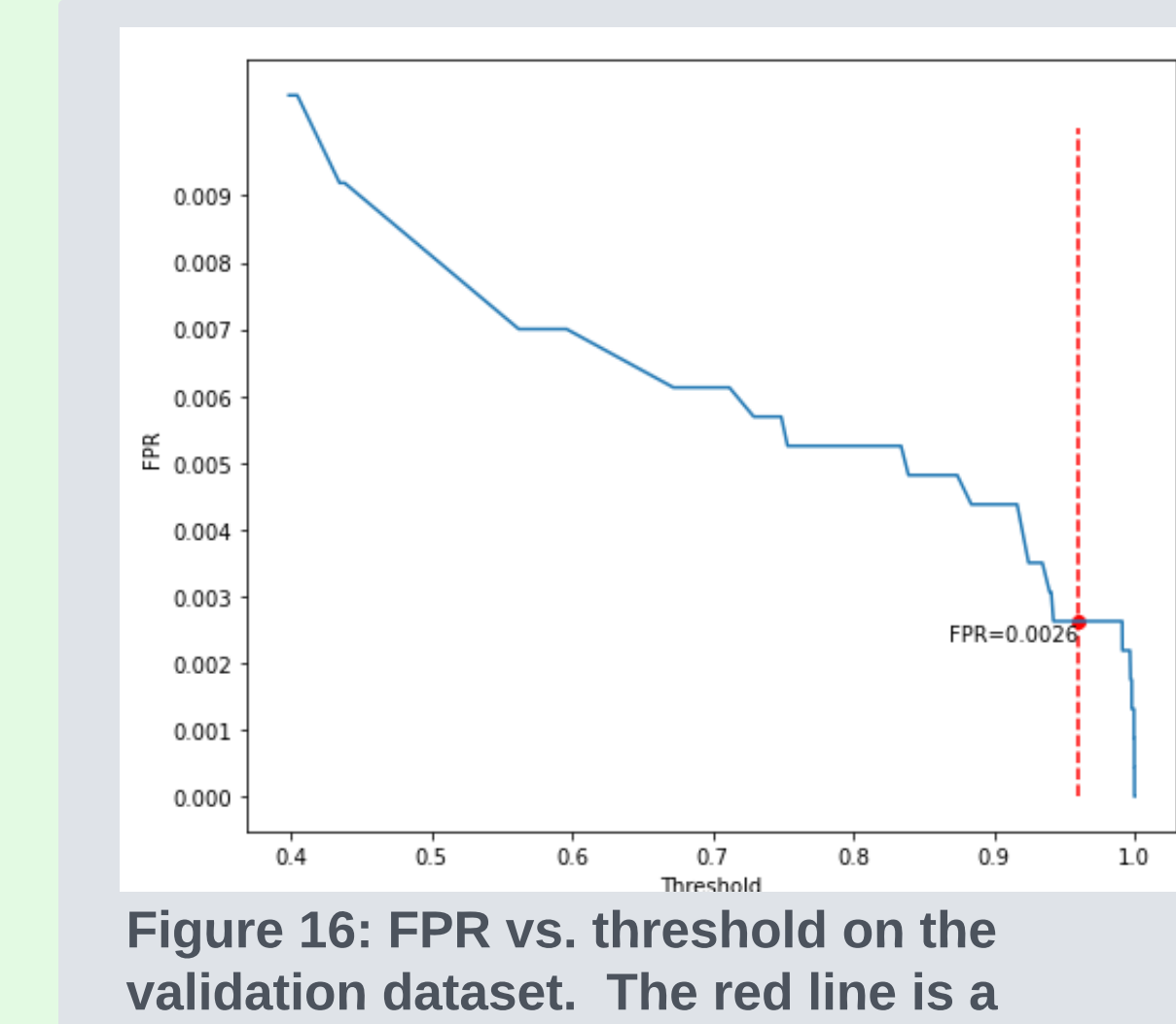


Figure 16: FPR vs. threshold on the validation dataset. The red line is a threshold value of 0.95.

Purity of muons is a priority for calibration. We choose a threshold of 0.95 to reduce FPR.

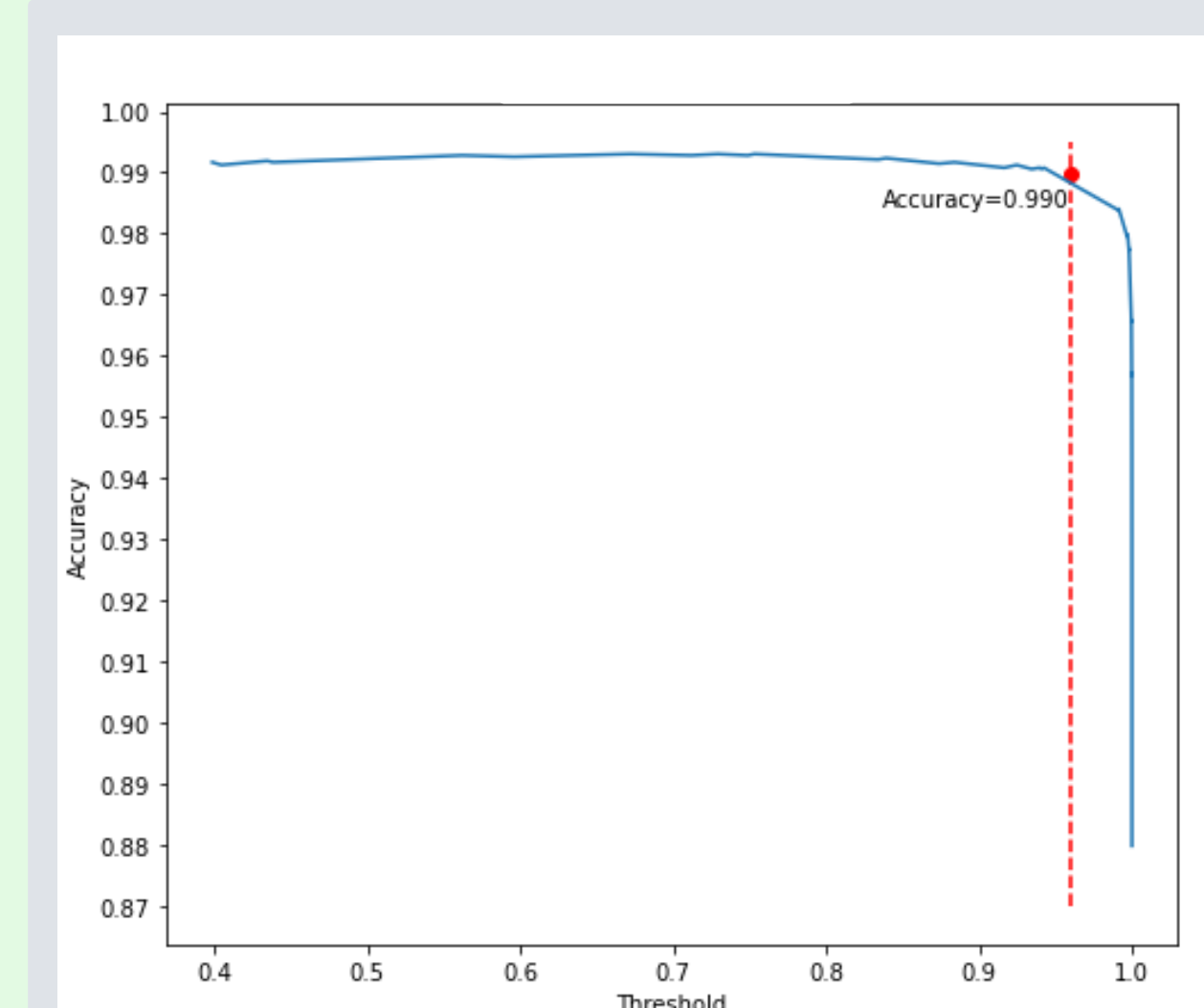


Figure 17: Accuracy vs. threshold plot. Accuracy is .990 for a threshold of 0.95 against the validation set.

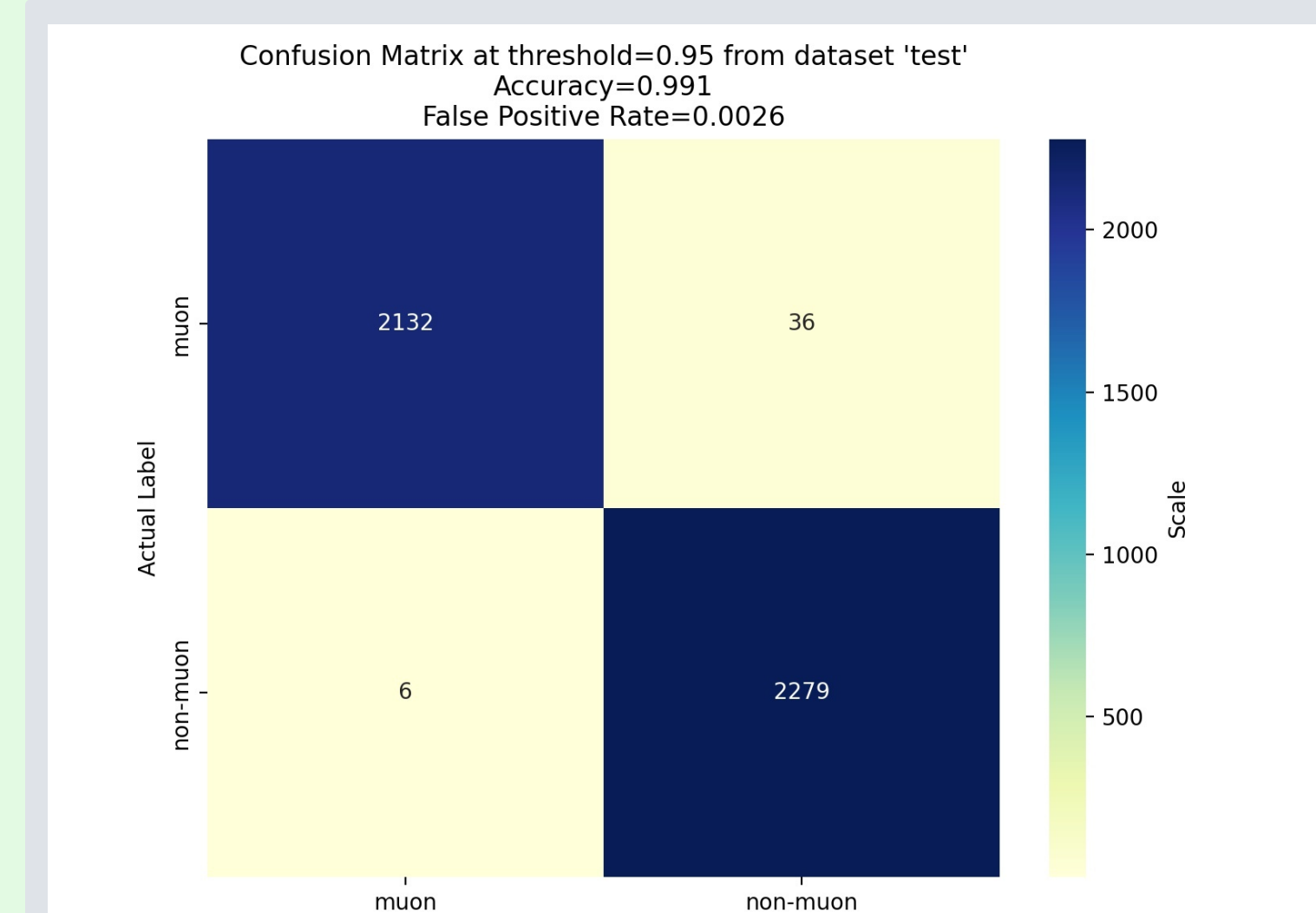


Figure 18: Confusion matrix, FPR and accuracy for trained simple CNN against the test dataset

	Flanagan with VGG16	Simplified CNN
FPR	0.0029	0.0026
Accuracy	0.997	0.991

Table 1: FPR and accuracy of our simple CNN vs. results by Flanagan using VGG16.

Source: [2]

Existing Method	Simplified CNN
TBD	TBD

Table 2: Number of muons identify by the existing method vs. our simplified CNN from a 200K VERITAS image dataset

Source: [2]

## Conclusions

- The FPR and Accuracy for CNN based muon identification achieved by Flanagan can be achieved with a 26x reduction in trainable parameters and 3x reduction in model layers. This simpler model reduced training time by 10x on MSI. Using a simpler model is one strategy for model generalizability [7].
- We anticipate being able to show that our simpler CNN is able to identify more muons than the existing method.
- Muon fitting can be achieved against the larger and more diverse set of muon images identified by our CNN. This includes fitting truncated muons as well as muons with non-muon signal in the image.
- We anticipate being able to show that our pipeline produces a larger quantity of and diversity of calibration-suitable muons.

## References

- [1] Q. Feng and J. Jarvis, "A citizen-science approach to muon events in imaging atmospheric Cherenkov telescopes: the muon hunter," 2017. [Online]. Available: <https://arxiv.org/abs/1708.04929>
- [2] K. Flanagan, "Identifying man-made cherenkov ring images in veritas data using convolutional neural networks," September 2020.
- [3] R. Bird, M. K. Daniel, H. Dickinson, Q. Feng, L. Fortson, A. Fumia, J. Jarvis, R. Mukherjee, R. Ong, S. Salich, and D. T. Smith, "The muon hunter: a zooniverse project," 2018. [Online]. Available: <https://arxiv.org/abs/1802.08909>
- [4] O. Catalano, M. Di Susto, T. Mino, G. Cusumano, M. Maccarone, and C. Pareschi, "Volume muon imaging using cherenkov telescopes," *Nuclear Instruments and Methods in Physics Research Section A: Accelerators, Spectrometers, Detectors and Associated Equipment*, vol. 902, pp. 1–6, 2018. [Online]. Available: <https://doi.org/10.1016/j.nima.2018.01.002>
- [5] J. Holder, R. Atkins, H. Badran, G. Hajjoude, S. Mekhora, J. Parker, C. Donahue, O. Catalano, C. Doku, A. Falcone, S. Fegan, J. Finley, P. Fortson, L. Fortson, K. Gibbs, G. Gilardoni, O. Gladwell, J. Grabe, K. Guettler, G. Gyuk, J. Hall, D. Hanna, R. Higley, J. Holden, J. Holden, J. Knapp, H. Krawczynski, J. Krennrich, M. Lang, S. Leibohm, L. Linson, J. Little, J. Kolodis, H. Krumholz, J. Krennrich, M. Lang, S. Leibohm, L. Linson, D. Little, J. Parker, H. Pohl, J. Quillian, K. Quillian, P. Quillian, L. Rizzo, H. Rizzo, D. Pritchard, J. Pritchard, S. Sledge, D. Steele, S. Swartz, A. Syson, J. Toner, L. Vakkarel, V. Vassiliev, and J. Walker, "Volume muon imaging using the VERITAS atmospheric Cherenkov telescope," *Astroparticle Physics*, vol. 23, no. 6, pp. 391–401, jul 2006. [Online]. Available: <https://doi.org/10.1016/j.astropartphys.2006.04.002>
- [6] M. F. L'Amoura, "Chapter 16 - cherenkov radiation," in *Radioactivity (Second Edition)*, ed. M. F. L'Amoura, Boston: Elsevier, 2016, pp. 547–570. [Online]. Available: <https://doi.org/10.1016/B978-0-12-800853-1.00016-1>
- [7] F. Maleki, K. Owens, K. Najian, B. Vergani, C. Reinhold, and R. Vergani, "Overview of machine learning part I: Fundamentals and classic approaches," *NeuroImage Clinics of North America*, vol. 30, no. 4, pp. e17–e32, 2020. machine Learning And Other Artificial Intelligence. Available: <https://doi.org/10.1016/j.nic.2019.101809>